A three-dimensional histological atlas of the human basal ganglia. II. Atlas deformation strategy and evaluation in deep brain stimulation for Parkinson disease

Clinical article

Eric Bardinet, Ph.D.,[1,8] Manik Bhattacharjee, R.I.,[1] Didier Dormont, M.D.,[1,2]
Bernard Pidoux, M.D., Ph.D.,[3] Grégoire Malandain, Ph.D.,[7]
Michael Schüpbach, M.D.,[4,5,9] Nicholas Ayache, Ph.D.,[7] Philippe Cornu, M.D.,[6,9]
Yves Agid, M.D., Ph.D.,[4,5,9–11] and Jérôme Yelnik, M.D.[9–11]

[1]Centre National de la Recherche Scientifique, Unité Propre de Recherche 640, Laboratoire de Neuroscience et Imagerie Cognitive, Paris; Départements de [2]Neuroradiologie, [3]Neurophysiologie, [4]Centre d'Investigation Clinique, [5]Fédération de Neurologie, and [6]Neurochirurgie, CHU Pitié-Salpêtrière, Paris; [7]Projet ASCLEPIOS, INRIA, Sophia-Antipolis; [8]Centre de Neuro-Imagerie de Recherche, [9]Hôpital de la Salpêtrière, Paris; [10]Institut National de la Santé et de la Recherche Médicale U679, Neurologie et Thérapeutique Expérimentale, Paris; and [11]Université Pierre et Marie Curie, Paris, France

Object. The localization of any given target in the brain has become a challenging issue because of the increased use of deep brain stimulation to treat Parkinson disease, dystonia, and nonmotor diseases (for example, Tourette syndrome, obsessive compulsive disorders, and depression). The aim of this study was to develop an automated method of adapting an atlas of the human basal ganglia to the brains of individual patients.

Methods. Magnetic resonance images of the brain specimen were obtained before extraction from the skull and histological processing. Adaptation of the atlas to individual patient anatomy was performed by reshaping the atlas MR images to the images obtained in the individual patient using a hierarchical registration applied to a region of interest centered on the basal ganglia, and then applying the reshaping matrix to the atlas surfaces.

Results. Results were evaluated by direct visual inspection of the structures visible on MR images and atlas anatomy, by comparison with electrophysiological intraoperative data, and with previous atlas studies in patients with Parkinson disease. The method was both robust and accurate, never failing to provide an anatomically reliable atlas to patient registration. The registration obtained did not exceed a 1-mm mismatch with the electrophysiological signatures in the region of the subthalamic nucleus.

Conclusions. This registration method applied to the basal ganglia atlas forms a powerful and reliable method for determining deep brain stimulation targets within the basal ganglia of individual patients.
(DOI: 10.3171/2008.3.17469)

Key Words • **atlas registration** • **basal ganglia** • **deep brain stimulation**

I n this paper we describe the adaptation of an atlas of the human basal ganglia to the identification of deep brain structures in individual patients. The atlas was developed and evaluated in the clinical context of DBS, and was conceived as a set of 3D histological structures that can be adjusted to fit the brains of different patients.

We believe this atlas to be applicable to any research experiment involving brain imaging.

Our objective was to develop an atlas that would combine histological, functional, and MR imaging information derived from a single postmortem brain specimen. Magnetic resonance imaging allowed coregistration of all atlas data in the MR imaging space and construction of truly 3D histological surfaces. In addition, MR imaging was also used for the transfer of the atlas data onto the MR images obtained in individual patients, and image-processing algorithms were developed to automate this process. In this paper, we describe our translation

Abbreviations used in this paper: AC-PC = anterior commissure–posterior commissure; DBS = deep brain stimulation; PD = Parkinson disease; ROI = region of interest; RU = red nucleus; SN = substantia nigra; STN = subthalamic nucleus; SW = Schaltenbrand and Wahren.

strategy, and evaluate its utility in patients with PD who underwent DBS treatment. Comparisons with intraoperative electrophysiological recordings and previous atlas studies are included.

Methods

The successive steps of the atlas construction have been published previously.[39] Briefly, a brain obtained at autopsy was subjected to MR imaging (T1- and T2-weighted sequences at 1.5-T strength) 35 hours after death. The brain was then extracted from the skull and separated into its 2 hemispheres; the left hemisphere was cut into 1.5-cm-thick blocks that were cut into 70-μm-thick coronal sections. Among the 800 sections obtained, 80 were stained with the Nissl technique, and 80 were stained with calbindin. The contours of the cerebral regions were traced under microscope observation, and atlas data were coregistered. Initial atlas contours were optimized through a double process of multimodal and 3D validation. The resulting atlas surfaces represent the best compromise between histological truth and 3D anatomical consistency.

In the present study, we explain the strategy used to adapt atlas data to individual patient anatomy, including forward and backward registration. This procedure is then evaluated along 3 different axes: evaluation of the deformation, comparison with intraoperative electrophysiology findings, and comparison with previous atlas studies in patients with PD. Comparison with intraoperative electrophysiology findings was considered a pivotal validation criterion as it allowed a direct comparison between independently acquired histological and electrophysiological data in the identification of deep brain structures at the same level of resolution.

Atlas Adaptation

Forward Registration. The 3D atlas of the basal ganglia structures is adapted to the brain of a given patient by automatic registration of the T1-weighted MR images obtained in the patient with the atlas postmortem T1-weighted MR images. Figure 1 illustrates the hierarchical framework that has been implemented. First, a global registration consisting of a rigid transform completed by an isotropic scaling factor is computed on the entire head. Then nonrigid (affine) registration is performed between atlas and patient ROIs. These ROIs incorporate the basal ganglia of the left hemisphere (dorsoventral limits: corpus callosum, pons; mediolateral limits: midsagittal plane, Sylvian fissure; anteroposterior limits: corpus callosum). The atlas ROI was defined and extracted from the atlas MR images once and for all, and the same ROI is automatically extracted on the globally registered patient images. To fit the atlas, which is built on the left hemisphere of the postmortem specimen, to the patient's right hemisphere, the same procedure is applied, preceded by a flip along the midsagittal plane of the patient's MR images. The resulting transformation matrices, 1 per hemisphere, are applied to atlas structures thus yielding to their best fit to both hemispheres of the patient's brain. All registrations are performed by applying an intensity-based robust multiscale block-matching algorithm (for details, see *Appendix* in the article by Yelnik et al.[39]).

In summary, atlas surfaces are adapted automatically and independently to the right and left hemispheres of any patient's brain using nonrigid transformations based on iconic registrations.

Backward Registration. The forward transformations can also be inverted, allowing transfer of patient information into the atlas geometry. We refer to this procedure as patient data normalization in the atlas space. The data subject to normalization are primarily the MR images, but all of the other data associated with the patient's MR images also is included. In patients undergoing neurostimulation, this includes positions of electrode active contacts or electrophysiological microelectrode recording data. Normalization of patient data into the atlas space is the fundamental tool that will enable the study of a series of patients, by back-projecting and assembling all of their data into a single geometry, thus allowing visualization, comparison, and statistical analysis.

Evaluation of Atlas Adaptation

The Salpêtrière Group. Atlas evaluation was performed in 2 series of patients: a consecutive series of 10 patients who underwent surgery in 2004, and a retrospective study in 10 patients with PD from whom a systematic anatomoclinical correlation based on the SW atlas[33] had previously been conducted.[40]

The stereotactically guided implantation of DBS electrodes in the Salpêtrière group, previously described in detail,[2] is briefly summarized, focusing on aspects relevant to the present study.

Preoperative target localization is based exclusively on stereotactic MR images, including T1- and T2-weighted images (voxel sizes 0.94 × 0.94 × 1 mm and 1.1 × 1.1 × 1 mm, respectively). Magnetic resonance imaging is performed the day before surgery with a General Electric 1.5-T MR imaging unit equipped with an MR imaging-compatible Leksell G stereotactic frame (Elekta). The parameters of the T2-weighted coronal acquisitions were optimized (reduced bandwidth) to yield a good contrast in the STN region. The coordinates of the STN are determined from the T2-weighted images and recorded on the stereotactic T1-weighted images. The trajectory, determined using stereotactic software, is defined by the stereotactic coordinates of the STN and 2 angles that determine the position of the arch holding the stereotactically guided microelectrode holder device and the position of the device on the arch.

During surgery, target localization is refined by microelectrode recordings. Electrophysiological recordings are performed along 2–5 parallel trajectories, 1 central and 4 peripheral, each situated 2.35 mm from the central trajectory that targets the predetermined STN coordinates. The microelectrodes are then inserted into guiding tubes aligned through a gun affixed to the Leksell stereotactic frame and hydraulic micrometer drive. Exploration proceeds from 5-mm above to 10-mm beyond the predefined target. Once the optimal site for implantation is chosen, the microelectrodes are removed and a quadripolar DBS electrode (3389, Medtronic Inc.) is inserted, which contains 4 discrete contacts, numbered 0–3 from
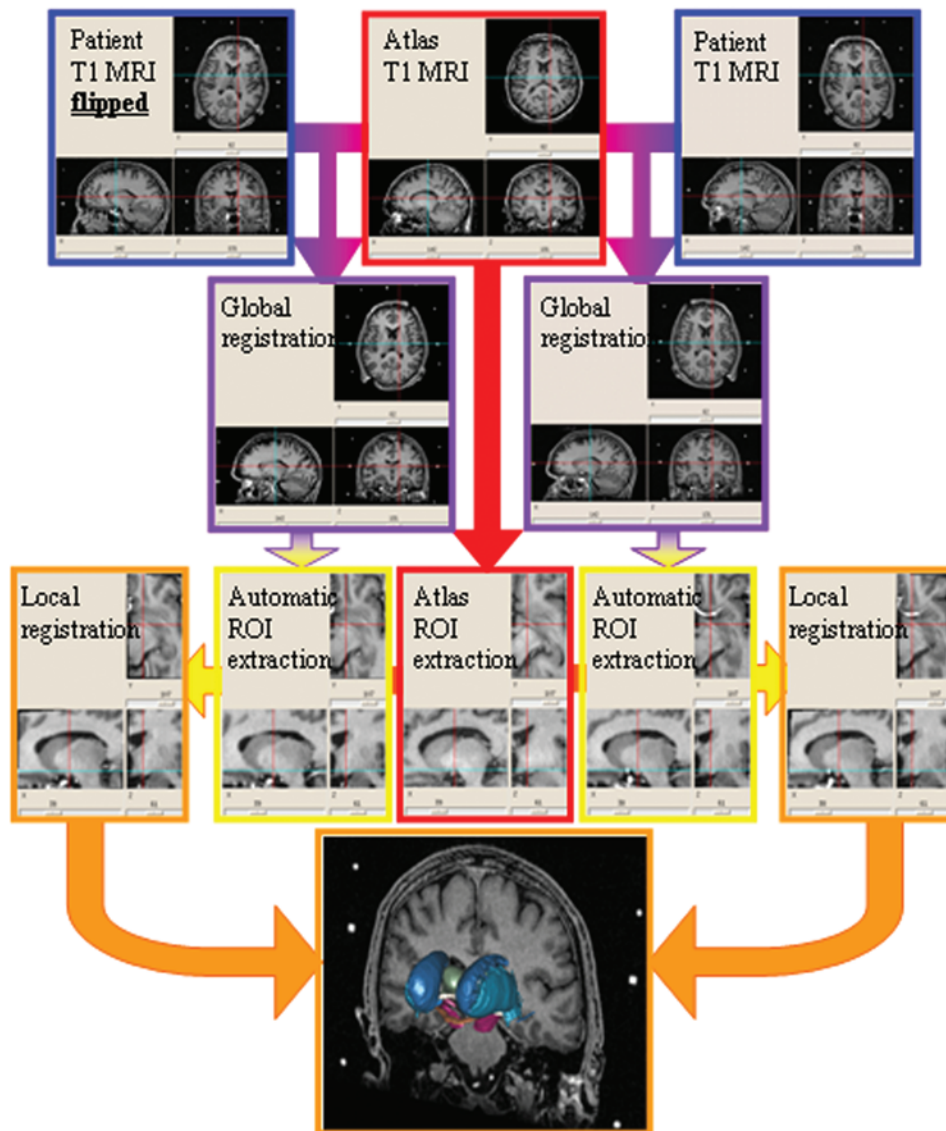
Fɪɢ. 1. Flow chart demonstrating the atlas MR imaging-based hierarchical deformation process. Each hemisphere *(blue boxes, first row)* is processed independently. Global registration *(purple boxes, second row)* with the atlas MR images *(red box, first row)* is followed by automatic ROI extraction *(yellow boxes, third row)* and local registration *(orange boxes, third row)*. The atlas ROI incorporating the basal ganglia has been extracted once and for all. For the right hemisphere *(left side* of the figure), the MR image is flipped along the anteroposterior axis before global registration. The resulting transformations are applied to the original atlas surfaces, resulting in surfaces adapted to the patient's brain *(orange box, last row).*

most ventral to most dorsal that are 1.3 mm in diameter, 1.5 mm in length, and 0.5 mm apart.

Electrode placement is controlled on MR images conducted the day after stereotactic implantation by using the same acquisition procedure as that in the preoperative step. Postoperative MR imaging strictly respected the recommendations of Medtronic for DBS protocols, particularly the specific absorption rate limitations and the use of a transmit/receive head coil. Patients who have recently undergone an operation now undergo CT scanning to avoid the possible side effects of postoperative MR imaging.

Evaluation With Standardized Visual Inspection. The result of atlas adaptation to a patient's brain is first evaluated by comparing the atlas contours of the structures that

are easily identifiable on T1-weighted MR images with the corresponding gray level regions on 3 orthogonal AC-PC standard planes (sagittal, coronal, and axial). Structures that are at least partially visible include the head of the caudate nucleus, the anterior and medial parts of the putamen, the lateral border of the cerebral peduncle, the anteroventral part of the optic tract and the medial border of the thalamus, including the habenula. This inspection allows a rapid but accurate evaluation of the degree of adjustment between the atlas contours and MR imaging results in each patient. Optimized T2-weighted MR images provide good contrast (hypointensities) in the STN region, which can be used to help define the preoperative target.[2] Visual inspection of the RU, SN, and STN, of particular interest for DBS

in patients with PD, is performed with T2-weighted MR images. Preoperative T2-weighted MR images are coregistered with the preoperative T1-weighted MR images (used to adapt the atlas to the patient's anatomy) with the same registration algorithm as that used for atlas deformation, allowing comparison of the STN, SN, and RU contours with the corresponding hypointense areas.

Evaluation by Averaging Spatially Normalized Images. All T1-weighted MR images were spatially normalized in the atlas space by using the atlas–patient MR imaging registration transformations. Intensity normalization was then performed by simple adjustment of the mean and standard deviation values of the individual histograms to compensate for the global intensity difference that may occur from one acquisition to the other. The normalized images were then superimposed to yield an average MR image. The rationale for this evaluation procedure is that consistent back-projections of patient MR images into the atlas space should result in a sharper average image. The same process was also performed with AC-PC linear normalization only (realigning all MR images along their automatically computed[31] midsagittal planes, and applying a linear transformation along the anteroposterior axis) to assess the improvement induced by atlas normalization.

Although qualitative, these procedures are very informative and considered important as they allow an evalua-tion of the atlas deformation either on an individual patient to test the accuracy of its adaptation in the particular patient, or globally within a series of patients to test the robustness and reproducibility of the deformation procedure.

Comparison With Intraoperative Microelectrode Recordings

The aim of this evaluation procedure was to compare, both qualitatively and quantitatively, the identification of the STN and surrounding structures using 2 independent methods: the adaptable 3D atlas and intraoperative electrophysiology. The first method was based on the deformation of our 3D atlas according to preoperative stereotactic 3D T1-weighted MR images; the second was based on electrophysiological recordings obtained during DBS surgery in the Salpêtrière group.

Electrophysiological signals, recorded every 0.5 mm during the intraoperative exploration, were interpreted by an electrophysiologist. The data consisted of positions in the stereotactic space (expressed as depth values in μm along the electrode trajectory) associated with a "signature" such as the STN, SN, zona incerta, or thalamus identification based on discharge frequency, pattern, and the electrophysiological level of activity (scaled from 1 to 4). Some positions do not have a signature because the electrophysiological signal was undetectable or unclear.
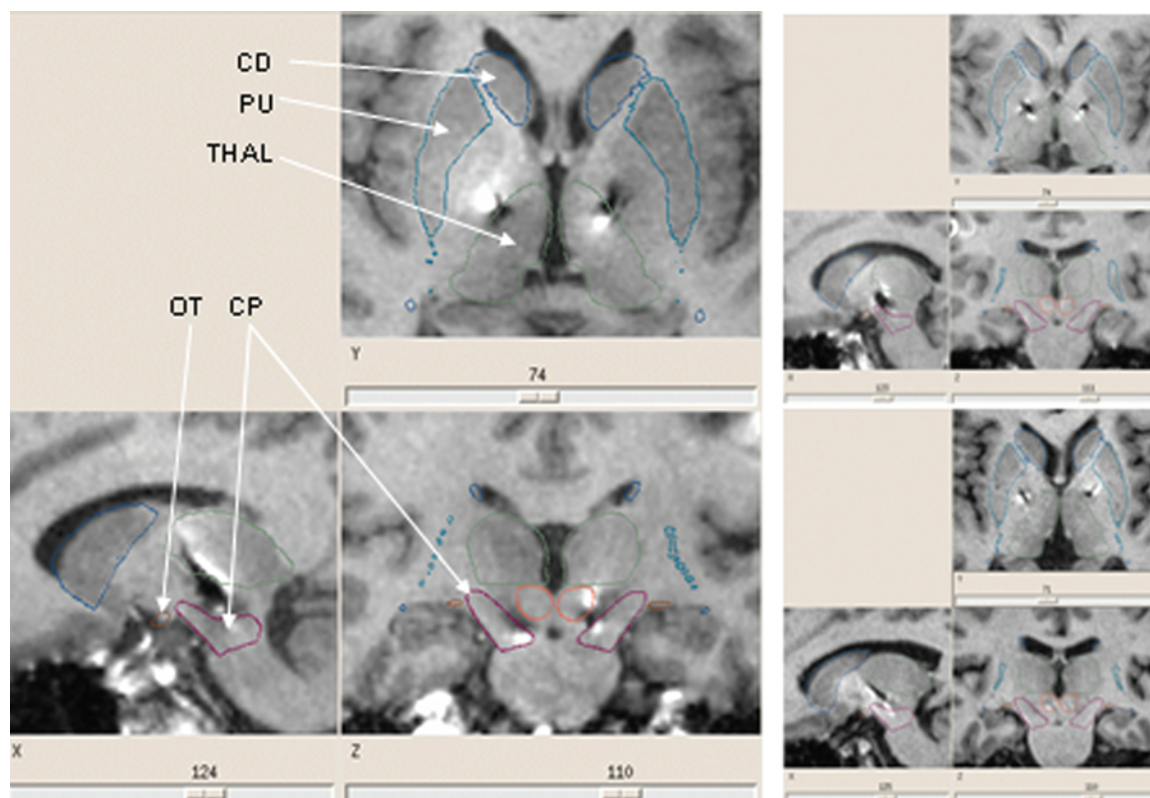

Fig. 2. Standardized visual inspection of deformed atlas structures in T1-weighted MR images. Postoperative MR images obtained in 3 patients are shown with superimposed atlas structures. The MR images were resliced along the AC-PC plane together with the contours of atlas structures visible on 3 orthogonal standard planes (sagittal, coronal, and axial): head of the caudate nucleus (CD), anterior and medial part of the putamen (PU), lateral border of the cerebral peduncle (CP), anteroventral part of the optic tract (OT), and medial border of the thalamus including the habenula (THAL). Note the close correspondence between the MR images and the atlas contours.

Deformation and evaluation of a 3D basal ganglia histological atlas

Three steps were necessary to compare these data with the deformed atlas defined on the MR images obtained in the patient. First, the stereotactic frame was automatically extracted from the preoperative 3D T1-weighted MR images obtained in the patient, by thresholding and connected components analysis. The frame was then rigidly registered with a binary image of the Leksell frame. This provided a transformation, which allowed insertion of the interpreted electrophysiological localizations, expressed with reference to the stereotactic frame, on each patient's MR images. Each electrophysiological recording was encoded as a sphere with a color and diameter corresponding to the signature and level of activity, respectively.

To compare atlas-based localizations with the signatures provided by the electrophysiological recordings, all recorded positions were examined through step-by-step rotations in a 3D viewer to determine whether or not the signatures matched the atlas anatomy. The number of correct and incorrect matches was recorded. Because electrophysiological activities were recorded every 0.5 mm, the distance between a mismatched position and the atlas-based limit of the corresponding structure could be determined by counting the number of spheres by which they were separated.

Comparison With Previous Atlas Studies

The goal of this third evaluation procedure was to compare the 3D atlas to the atlas most frequently used by neurological and neurosurgical teams, the SW atlas.[33] This comparison was based on 2 approaches.

First, a direct comparison was made between the anatomical contours provided by the 2 atlases. The 3D atlas MR images were reformatted in the same axial plane as the axial SW atlas, and the 3D surfaces were sliced in this orientation. The SW atlas was adapted to the MR images by applying the semiautomated coregistration method developed by one of the authors (J.Y.).[40] As a result, the sections of the SW atlas and our 3D atlas could be seen juxtaposed at the same level of the MR imaging.

Second, we compared the anatomical localization of DBS electrodes obtained with the SW atlas and that obtained with the same data using the 3D atlas. These data were taken from a clinically validated retrospective study by the Salpêtrière group.[40] In this study, anatomical localization of the 4 contacts of each electrode, tested separately by the clinicians, was determined on postoperative MR images using the semiautomated coregistration method with which the digitized 2D contours of the SW book atlas are adapted linearly to a given patient's postoperative MR images.[40] With our 3D atlas, contacts were identified in 3D by reslicing the original postoperative MR images along the electrode axes and placing a template of the electrode at the center of the MR imaging artifact.[30,40] Using this method, the position of the 4 contacts could be accurately defined. The 3D atlas was then automatically adapted to the patient's brain, allowing localization of the contacts relative to the histological structures provided by the atlas.

It is worth noting that if a scanner acquisition is the only postoperative image available (due to safety issues, this is usually the case at our institution), the 3D atlas can still be used for contact localization. The scanner, used to identify the contacts, is rigidly registered on the preoperative MR images that serve as the reference images for atlas adaptation.

Results

Evaluation of Atlas Adaptation

Standardized Visual Inspection. Once the atlas was adapted to the patient's brain, standardized visual inspection was performed in 3 orthogonal planes of the T1-weighted MR images obtained in the AC-PC reference system. Each plane was selected to optimize comparison between T1-weighted MR imaged structures and the corresponding atlas contours. The axial planes allowed the head of the caudate nucleus, the putamen, and the medial border of the thalamus, including the habenula, to be checked. Coronal planes were chosen to inspect the optic tracts and lateral borders of cerebral peduncles. These structures appeared in the sagittal planes, which also included the body of the caudate nucleus. Figure 2 shows standardized views of postoperative T1-weighted MR images in 3 patients, illustrating a good correspondence between T1 contrast and atlas contours. In particular, excellent correspondence was observed in the subthalamic region (SN, STN, RU, and cerebral peduncle) in which mismatches, of the order of 1 pixel ($\sim$ 1 mm), were rare (for example, the cerebral peduncle in Fig. 2). Weaker correspondences (1–3 pixels) could be observed for the anterior parts of the caudate nucleus or putamen.

Two coronal slices of T2-weighted MR images perpendicular to the AC-PC line were studied: 1 through the center of the RU, and 1 anterior to the RU where the hypointense signal is expected to correspond to both the RU and STN. Figure 3 shows these 2 slices in 2 patients, with and without atlas contours and demonstrates a very good correspondence between the zones of hypointense signal and the expected anatomical contours of SN, STN, and RU. In particular, the limit between the hypointense SN and the adjacent cerebral peduncle is localized accurately.

Average of Spatially Normalized Images. Averaged MR images obtained through AC-PC and atlas-based normalizations of all the MR imaging data used in this study (obtained in 20 patients) are shown as 2 series of perpendicular standard planes in Fig. 4. Overall, visual inspection reveals that atlas-based normalization leads to a globally sharper average image than AC-PC linear normalization. This is particularly obvious at the border between the corpus callosum, lateral ventricle, and caudate nucleus. The contours of the striatum (caudate nucleus, putamen, and nucleus accumbens) are also greatly improved by atlas normalization in the axial, sagittal, and coronal planes. Finally, the ventral extension of the putamen seen in posterior coronal sections becomes apparent with the atlas normalization whereas it is invisible with AC-PC normalization.

Comparison With Intraoperative Microelectrode Recordings

Superposition of atlas-based STN surfaces and encoded microelectrode recording data are illustrated in 1 patient for whom exploration was performed in 2 trajec-
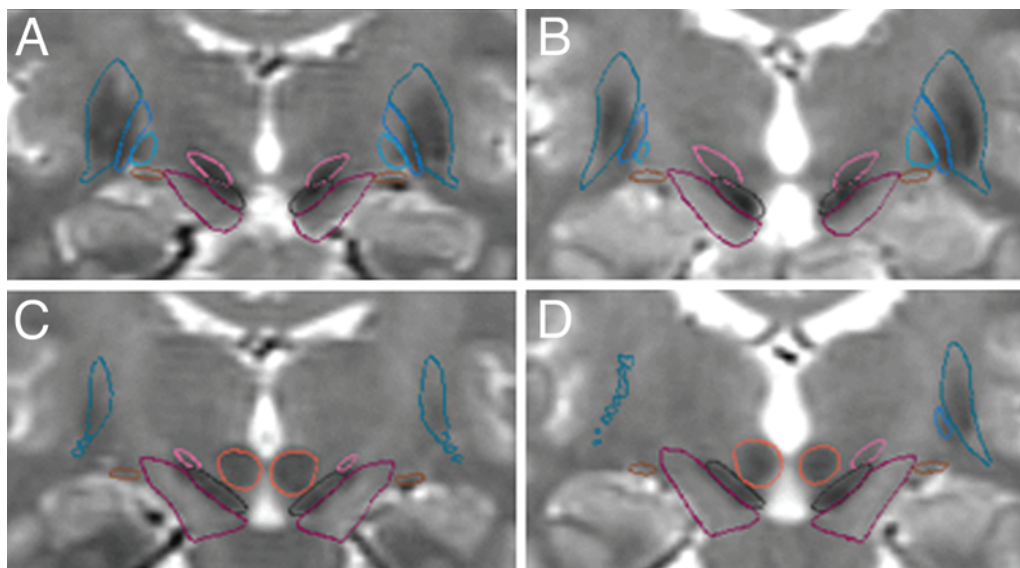
Fɪɢ. 3. Standardized visual inspection of deformed atlas structures in T2-weighted MR images. The T2-weighted MR image was automatically coregistered with the T1-weighted MR image (used to deform the atlas), thus allowing comparison of STN *(pink)*, SN *(black)*, and RU *(red)* contours with hypointense areas. Images obtained in 2 patients are presented *(left and right boxes)*. For each case, 2 coronal slices are presented: 1 through the center of RU (C and D), and 1 anterior to RU (A and B). The contours of the putamen and globus pallidus are in *blue*, that of the cerebral peduncle in *fuchsia*.

tories for each hemisphere (73 recording localizations; Fig. 5). Step-by-step rotations in the 3D viewer revealed an almost perfect correspondence between electrophysiological STN and SN signatures and the atlas-based identification of the same structures. Counting of correct and incorrect matches showed that all electrophysiologically defined localizations corresponded to the expected atlas-defined structures, except for 2 low-intensity STN signatures, which were 0.5-mm (1 sphere apart) outside the STN surface.

In the complete series of 10 patients, 51 trajectories were studied (24 in the left and 27 in the right hemisphere), which provided 965 electrophysiological recordings among which 408 were identified as STN activity and 63 as SN activity by the electrophysiologist. All electrophysiological data were back-projected onto the atlas space and superimposed on the STN of the 3D atlas. The results for 1 hemisphere are shown in Fig. 5. Of the 408 STN recordings, 330 (81%) were included in the STN surface as defined by atlas adaptation, and 78 (19%) were not. Among the 564 recordings that were not labeled as STN activity, 434 (77%) were actually outside the STN and 130 (23%) were inside. Among the 63 SN recordings, 49 (78%) were included in the SN surfaces and 14 (22%) were not. The distance between a mismatched signature and the atlas-based localization was measured for all mismatches, which revealed that the worst mismatches extended over a maximum of 3 adjacent spheres (a distance of 1.5 mm). Most of the mismatch distances extended over 1 or 2 spheres, suggesting a 1-mm accuracy for the atlas-based localization of the STN.

Comparison With Previous Atlas Studies

Comparison between the SW atlas sections and the corresponding sections of our new 3D atlas is illustrated for 1 atlas level in Fig. 6. Overall, the 2 atlases were very similar, for example see the level at which the external and internal globus pallidus appeared along the dorsoventral axis, and the shape and localization of RU, STN, or SN contours in different axial sections. This similarity gives credibility to the contour tracing of both atlases. There were, however, noticeable differences between the 2 atlases related to the tracing of particular cerebral regions such as the zona incerta, the SN, and the cerebral peduncle, which are traced as open (thus incomplete) contours in the SW atlas and completely defined in our 3D atlas (Fig. 6). Also, to obtain a satisfactory adaptation of the SW atlas to MR images obtained in a patient (assessed by the contours of the putamen, fornix, mamillothalamic tract, and AC), it is necessary to place the midline of the atlas more lateral than the actual ventricle midline on the MR images. This is not the case with our 3D atlas, which is automatically adapted using MR imaging–based registration.

Comparisons with a previous anatomoclinical study[40] are illustrated in Figs. 7 and 8, and results of the automatic registration of our new 3D atlas are illustrated in Fig. 7. The 3D views in Fig. 8 demonstrate the back-projection of the 20 therapeutic contacts (10 on each side), which clearly reveal the position of all contacts within the STN. As a whole, automatic registration of the 3D atlas led to 14 therapeutic contacts within the STN versus 15 found with the semiautomated adaptation of the SW atlas.[40] Two contacts were located at the border of the STN with both methods. The other contacts were localized in the Forel field H2 (2 contacts vs 1 with the semiautomatic method), zona incerta (2 vs 1), and mesencephalic reticular formation (no contacts vs 1). As a whole, the automatic adaptation of the 3D atlas to patient images yielded results very similar to the semiautomated adaptation of the SW atlas; this provides an additional independent validation of the automatic adaptation of the 3D atlas and increases confidence in its clinical utility.
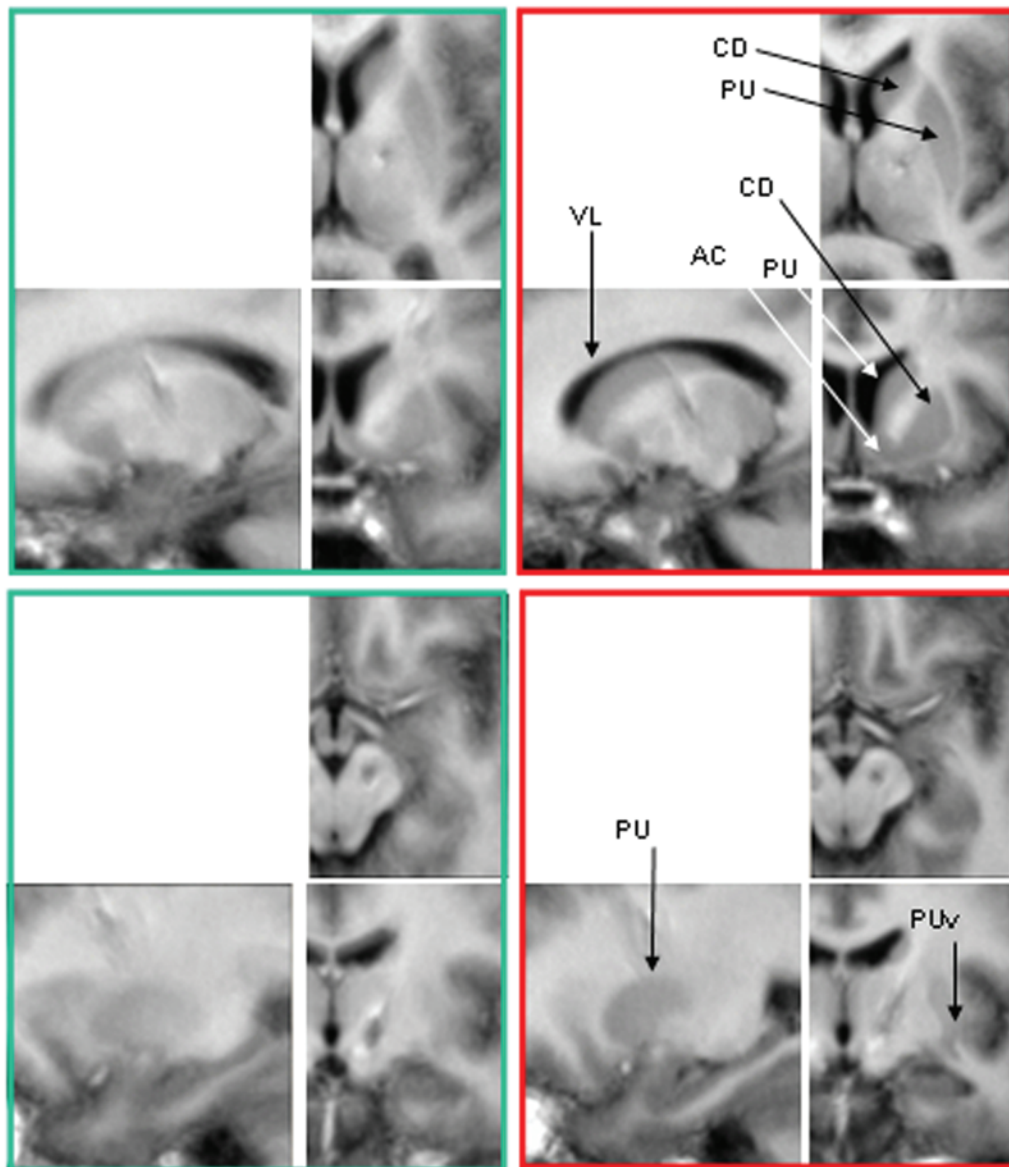
Fig. 4. Average of spatially normalized MR images obtained in the 20 patients analyzed in this study. The *green boxes* showing AC-PC normalization, and the *red boxes* showing atlas normalization. *Upper:* Anterior, medial, and dorsal slices. *Lower:* Posterior, lateral, and ventral slices. Only 1 hemisphere is presented (the atlas is deformed independently on the 2 hemispheres). Note that the contours of gray level areas are sharper with atlas normalization. AC = nucleus accumbens; PUv = ventral putamen; VL = lateral ventricle.

On the basis of these results, the 3D atlas and its adaptation procedure is both a robust and accurate method; it never failed to provide an anatomically reliable atlas-to-patient registration, which was most often excellent in the region of the STN.

Discussion

Our method allows the automatic application of a 3D histological atlas of the basal ganglia[39] onto any patient's brain. This is performed through a hierarchical registration framework (first global and then local) applied to the atlas and the patient's T1-weighted MR images, with each hemisphere mapped independently. This method has been evaluated on visual inspection of the deformation, comparison with the atlas-based mapping of the STN region with the identification of the same region on electrophysiological recordings, and comparison with previous atlas studies in patients with PD.

Comparison With Other Atlas-Based Approaches

Deep brain structures in individual patients can be identified using direct or indirect strategies. Direct methods identify structures on the MR images themselves,[1,4,12,14,21,29,34] but only the structures that are at least partially visible on MR images (for example the lateral ventricles, caudate nucleus and putamen, thalamus, and optic tract) can actually be identified with some certainty. One has proposed an orig-
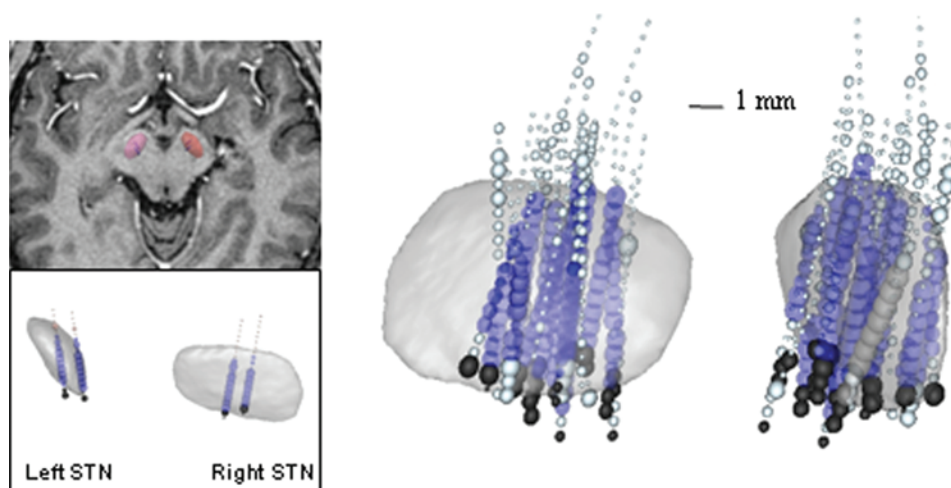
FIG. 5. Comparison between atlas-based STN delimitation and intraoperative microelectrode STN recordings. *Left:* Axial view of the patient's MR image *(top)* with left and right STN *(transparent pink)* and 73 recordings *(spheres)*, and enlargement *(bottom)* of the left and right STN superimposed with the recordings. *Right:* Back-projection in the atlas space of 965 microelectrode recordings obtained in 10 patients. *Dark blue spheres* correspond to STN recordings, *black* to SN, and *light blue* to unlabeled data. The STN is shown in 2 orthogonal rotations oriented along the principal axis. Note the good correspondence between the atlas STN and the *dark blue spheres*. The *black spheres* are ventral to the STN, in conformity with the ventral position of the SN.

inal alternative which consists of acquiring high-resolution, 4.7-T MR images of a postmortem, fixed brain specimen, analyzing the anatomy of the subthalamic region on MR images, and deriving a similar sequence applicable at 1.5 T in clinical conditions.[6] Indirect methods are based on high-resolution atlases adapted to a given patient's MR images.

With printed atlases,[19,22,33,37] adaptation must be done mentally by the atlas user. Printed atlases can also be digitized and interactively coregistered with the patient's images.[23,40] Better and more easily reproducible results are obtained with digital atlases, initially developed for educational purposes, and often available online or on CD-ROM. The Ta-
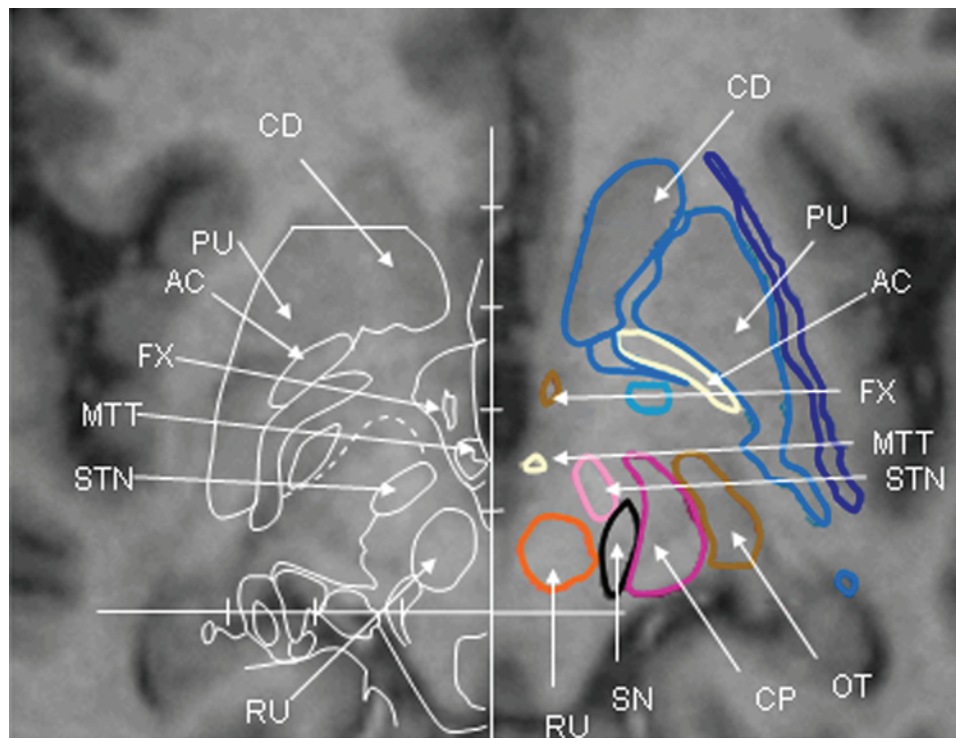

FIG. 6. Split MR image showing a comparison between the SW atlas and our 3D atlas. *Left:* One section of the axial SW atlas (PC: 6 mm) was adapted to the MR image of the 3D atlas. The corresponding contours, similar to those in the SW atlas, appear as *white tracings*. *Right:* The contours of the 3D atlas, obtained by automatic sectioning of the 3D surfaces, appear as *colored tracings*. Note that both atlases are globally similar but that the SN and cerebral peduncle are precisely delimited in the 3D atlas while they are not present or incompletely delimited in the SW atlas. FX = anterior column of the fornix; MTT = mamillothalamic tract; PU = putamen.
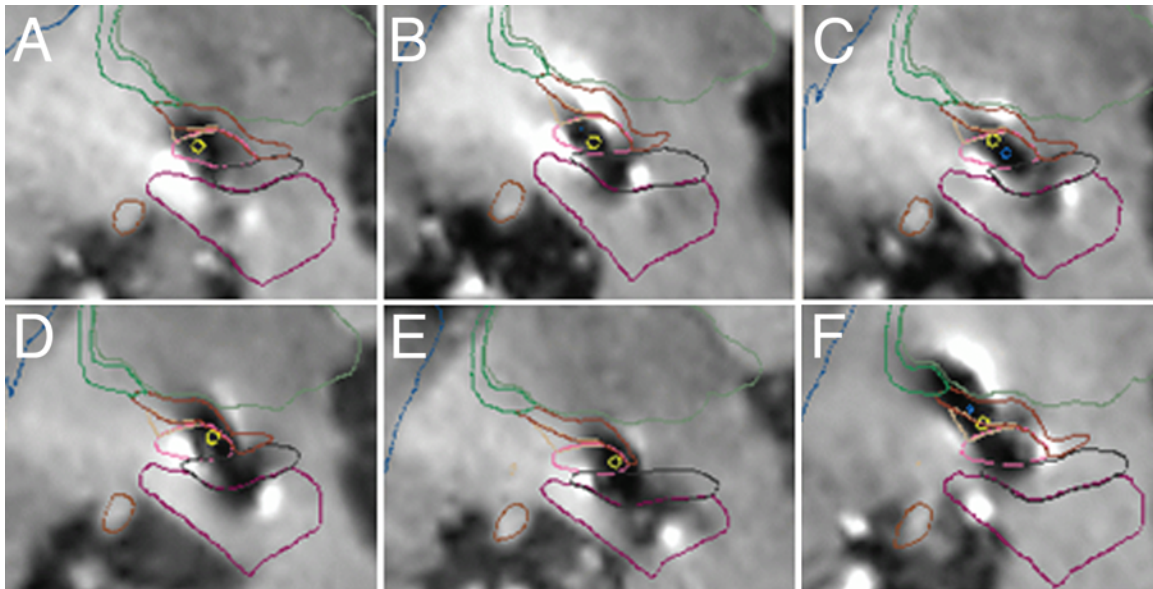
FIG. 7. Representative contact localization images obtained in the series of 10 patients with PD who underwent STN DBS. Sagittal slices of MR images obtained in 6 of these patients are illustrated. The therapeutic contact *(yellow)* is in the STN *(pink)* in the 5 first cases and at the limit between the zona incerta and Forel field H2 in the later case. Note that cerebral peduncle *(fuchsia)* and the optic tract *(brown)* of the 3D atlas are very tightly registered to the corresponding aspect of the MR imaging.

lairach Daemon, for example, is a digitized version of the Talairach and Tournoux atlas, the SPL Anatomy Browser permits navigation in a T1-weighted MR imaging volume in which brain regions were previously segmented, and the Nowinski Multimodal Atlas integrates digitized printed atlases into a common navigation tool. Probabilistic atlases have also been developed but these are mainly intended for work within the cortical sulci of the cerebral cortex.

Several groups have developed methods to adapt these atlases to individual patient anatomy using landmarks-based proportionality coefficients[23,27,28,38,41] or automatic registration with patient MR imaging acquisitions: for example, deformation of the Talaraich atlas based on cortical and ventricular contours,[13] an MR imaging-based deformable atlas for accurate radiotherapy planning,[3] and an elastic MR imaging registration of the Kikinis atlas.[9,17]
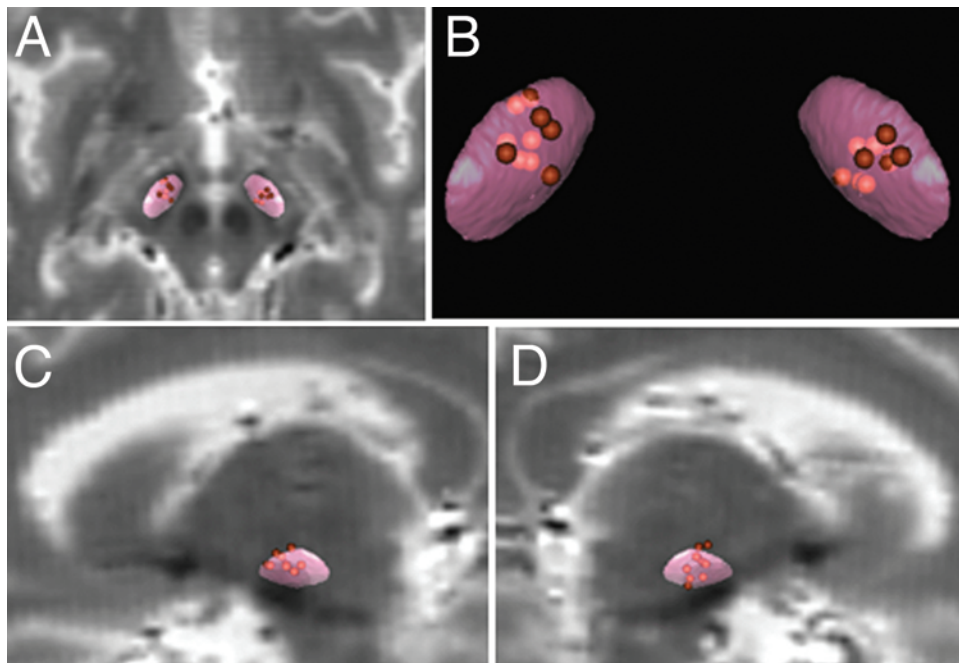

FIG. 8. Contact localization in the series of 10 patients with PD treated by STN DBS. The 20 contacts (10 on each side represented as *spheres*) were back-projected onto the atlas. A: The 2 STN *(pink)* are seen with an axial section of the T2-weighted MR images of the atlas. B: Closer view of the same STN. Contacts localized outside the STN are *dark colored*; those within the STN are *light colored*. C and D: Sagittal views of left and right STN with T2-weighted MR images of the atlas.

Two groups have developed computer-assisted methods for planning and guidance in DBS procedures that include atlases and are based on series of data collected in neurostimulated patients. Finnis and coworkers[11] and Guo et al.[15] built a multimodal functional database that incorporates spatially normalized collections of final surgical targets and electrophysiological recordings from previous patients as well as a volumetric digital atlas. This database is integrated into a visualization and navigation system that allows adaptation to individual patients by nonrigid registration. The volumetric atlas was built by digitizing the histological slices and contour tracings of the printed SW atlas, aligning the slices, interpolating the contours, and registering the resulting histological volume with average T1-weighted MR images by semiautomated landmark-based spline interpolation.[35] The computer-assisted system as a whole represents a useful tool for neurosurgical planning, but the accuracy of the volumetric atlas is limited to that of the axial SW atlas, which comprises only 20 sections with variable spacing (1–4 mm) and exhibits important 3D inconsistencies.[24] Moreover, the lack of MR images in the original SW atlas had to be overcome by spline interpolation with average in vivo MR images, a process that inevitably introduces inaccuracies to the volumetric atlas. D'Haese and coworkers[8] also developed a system for computer-assisted planning and guidance. No anatomical atlas was included in this system, the aim of which was to build purely functional maps of the areas of interest for targeting and guidance by spatially normalizing collections of data (electrophysiological recordings and optimal target points), including automatic analysis of the electrophysiological recordings.

Chakravarty and coworkers[7] recently proposed a 3D anatomical atlas for neurosurgical planning. The atlas was derived from a set of serial histological data. To overcome the lack of MR images of the brain specimen, pseudo-MR images were created from the reconstructed voxel-labeled atlas volume and used to adapt the atlas to any patient through nonrigid registration.

The specific quality of our present atlas is a unique combination of a histological level of resolution, inclusion of functional information based on calbindin staining, a large number of sections (160 sections with 0.35-mm intervals) and MR imaging acquisitions of the same specimen that allowed the construction of truly continuous 3D surfaces[39] and their automated adaptation to patients by MR image registration.

Atlas Deformation

Whichever atlas is used, atlas strategy requires the choice of a deformation method that allows the most reliable adaptation of the atlas to different brains, and conversely spatial normalization of patient data within the atlas space.

Spatial normalization can be performed in the Talairach AC-PC–based linear proportional system.[16,26,32,40] In each patient undergoing DBS, contact localization is expressed in the individual AC-PC–based reference system, while for group analysis, these data are normalized in a common reference frame by applying a linear normalization based on the AC-PC length,[16,32] a bilinear normalization (AC-PC length and height of the thalamus),[26] or a trilinear normalization based on multiple MR imaging landmarks.[40]

Spatial normalization can also be performed automatically by using image registration. In some studies, data related to a given patient are back-projected onto a normalized space by nonrigid registration of MR images.[7,8,11,15] With our 3D histological atlas, MR images were included in the construction of the atlas with the aim of adapting it to any patient's MR images by image registration. Two constraints had to be satisfied. First, the registration procedure had to be robust, parameter free, and relatively fast because the atlas is intended for use in clinical research. Second, because the atlas is composed of histological structures, registration had to produce anatomically plausible deformations at the level of histological definition. We started by testing nonrigid registration techniques based on whole-brain images.[5,36] These approaches, apart from being time-consuming, required the fine-tuning of a number of parameters to get the best compromise between goodness-of-fit and transformation regularity. The results of our experiments demonstrated that it was not possible to adjust the parameters to cope with our specific constraints; a satisfactory adaptation of the atlas to patient MR images was obtained only at the expense of anatomically implausible deformations. Because we were only interested in the basal ganglia structures, we then tested a nonrigid procedure initialized with a global (rigid and isotropic scale transformation) alignment of the images, and refined locally with affine transformations on automatically extracted ROIs. This ultimately produced 2 transformations, 1 per hemisphere. The algorithm, which was used for the global and local registration steps, is sturdy and reasonably fast (10 minutes for atlas–patient registration on a standard workstation).

Evaluation of Atlas Deformation

In all the patients included in this study, evaluation of atlas deformation by standardized visual inspection indicated very good results in a ventral region comprising the putamen and thalamus; the STN, SN, and RU nuclei; and the cerebral peduncle. Atlas-based contours were in close correspondence with gray level structures on the T1-weighted MR images. In some cases, dorsomedial contours, in particular the head of the caudate nucleus, could be less accurately registered, specifically in the presence of large lateral ventricles, but with the ventral region still being accurately registered. This proved the robustness of the registration algorithm, which ensures an accurate atlas-based mapping of the aforementioned ventral region, even in the presence of large lateral ventricles. Considering the highest mismatches that were observed between atlas-based contours and MR imaging–identifiable structures in the 20 patients, the accuracy of atlas-based mapping in this ventral region is of the order of 1 mm, which is comparable to the voxel size of the patients MR images.

Comparison with intraoperative microelectrode recording data was considered to be an important criterion for atlas validation because this approach, often used as the gold standard for STN identification at DBS centers, allowed comparison of 2 completely independent approaches to the identification of the STN at the same level of resolu-

Deformation and evaluation of a 3D basal ganglia histological atlas

tion, namely histological and electrophysiological. Microelectrode recording provides a very accurate intraoperative local identification of the brain nuclei crossed by the microelectrodes. As a whole, a very good correspondence (80%) was found between the present atlas-based STN identification method and microelectrode recording–based identification method performed by an electrophysiologist. Determination of the extent of mismatches between atlas-based localizations and electrophysiological signatures led to a finding of 1-mm accuracy.

Comparison with previous atlas studies was also considered crucial to validate our 3D atlas for 2 reasons. First, because the SW atlas is the most frequently used atlas in DBS, it seemed necessary to present both the similarities between our atlas and the SW atlas and some of the known inconsistencies of the latter. Second, it seemed pertinent to verify that some results previously validated in the Salpêtrière group study could also be obtained by applying this 3D atlas to the same MR imaging data. The first and most significant difference between the SW atlas and the 3D atlas is the number of sections available (for example, 20 sections are available in the axial series of the SW atlas), which is not predetermined in the current 3D atlas because the atlas structures consist of continuous surfaces. The number of sections can therefore be as high as needed for clinical or experimental protocols. Second, the 3D coherency of the contours of the original SW atlas was not verified during the construction of the atlas, leading to irregular 3D contours that cannot be sliced in other directions.[24,25] An example of this is the STN.[10] In the 3D atlas, the contours consist of 3D surfaces that can be sliced in any direction, either standard anatomical planes, or arbitrary oblique planes as is possible along electrode trajectories.

Comparison of our 3D atlas with a clinically validated published study has shown that previous results are reproducible with the present atlas. In a study conducted in 10 patients with PD, semiautomated registration based on the SW atlas led to 15 active contacts in the STN in the 10 patients (20 electrodes). After automatic registration of the 3D atlas, 14 active contacts were located in the STN. The similarity between the 2 sets of results suggests that atlas MR imaging registration is a reliable technique. The 1 contact difference is probably the result of differences in the quality of the 2 atlases. The SW comprises only 20 sections with variable spacing (1–4 mm), which means that the MR imaging sections corresponding to the position of a given contact had to be registered with the nearest, but often distant, section of the SW atlas.[40]

The positive results obtained with these 3 evaluation procedures (standardized visual inspection, comparison with microelectrode recordings, and comparison with previous atlas studies) prove that this 3D atlas and its image deformation procedure is a robust and accurate method. It is robust because atlas–patient registration never failed to provide anatomically reliable results, and accurate because anatomical structures in the subthalamic region can be identified with a 1-mm accuracy.

Our project is now to make this atlas available to as many users as possible. Three strategies are currently in process. First, the atlas will be integrated into the neuronavigation StealthStation commercialized by the Medtron-

ic company, which is in use at several DBS centers and which presently uses the SW atlas.[33] Second, we will make the main basal ganglia regions of the atlas available as a toolbox of labeled ROI volumes as it is presently the case for the AAL toolbox in the SPM software (http://www.fil.ion.ucl.ac.uk/spm/). Third, we are presently developing a stereotactic toolbox for BrainVisa software (freely available; http://brainvisa.info/index.html), which will be useful for research in the basal ganglia and for experimental targeting in DBS neurosurgery in general.

Conclusions

We have presented an automated procedure with which a 3D histological atlas of the basal ganglia can be adjusted to the anatomy of individual patients. This is performed by coregistration of the MR imaging T1-weighted image of the atlas specimen (postmortem acquisition before brain extraction) and that of the patient. We have evaluated this procedure using 3 different approaches: evaluation of the deformation itself, comparison with intraoperative microelectrode recordings, and comparison with previous atlas studies in patients with PD. These independent validation procedures revealed close correspondence between the present atlas strategy and previous procedures, in particular with regard to the delimitation of the STN.

On the basis of our results, we conclude that a 1-mm accuracy for target localization is achievable with this atlas. This atlas and the procedure we describe have the potential to become generally applicable clinical tools in DBS protocols and other clinical situations in which identification of the basal ganglia with a high degree of resolution is required. An additional application could be localization of the bold signal in functional MR imaging studies[18] or any other research experiment involving brain imaging.[20]

References

1. Barra V, Boire JY: Automatic segmentation of subcortical brain structures in MR images using information fusion. **IEEE Trans Med Imaging 20:**549–558, 2001
2. Bejjani BP, Dormont D, Pidoux B, Yelnik J, Damier P, Arnulf I, et al: Bilateral subthalamic stimulation for Parkinson's disease by using three-dimensional stereotactic magnetic resonance imaging and electrophysiological guidance. **J Neurosurg 92:**615–625, 2000
3. Bondiau PY, Malandain G, Chanalet S, Marcy PY, Habrand JL, Fauchon F, et al: Atlas-based automatic segmentation of MR images: validation study on the brainstem in radiotherapy context. **Int J Radiat Oncol Biol Phys 61:**289–298, 2005
4. Bueno G, Musse O, Heitz F, Armspach JP: Three-dimensional segmentation of anatomical structures in MR images on large data bases. **Magn Reson Imaging 19:**73–88, 2001

5. Cachier P, Bardinet E, Dormont D, Pennec X, Ayache N: Iconic feature based nonrigid registration: the PASHA algorithm. **Comput Vis Image Underst 89:**272–298, 2003

6. Caire F, Derost P, Coste J, Bonny JM, Durif F, Frenoux E, et al: [Subthalamic deep brain stimulation for severe idiopathic Parkinson's disease. Location study of the effective contacts.] **Neurochirurgie 52:**15–25, 2006 (Fr)

7. Chakravarty MM, Bertrand G, Hodge CP, Sadikot AF, Collins DL: The creation of a brain atlas for image guided neurosurgery using serial histological data. **Neuroimage 30:**359–376, 2006

8. D'Haese PF, Cetinkaya E, Konrad PE, Kao C, Dawant BM: Computer-aided placement of deep brain stimulators: from planning to intraoperative guidance. **IEEE Trans Med Imaging 24:**1469–1478, 2005

9. Dawant BM, Hartmann SL, Thirion JP, Maes F, Vandermeulen D, Demaerel P: Automatic 3-D segmentation of internal structures of the head in MR images using a combination of similarity and free-form transformations: part I, methodology and validation on normal subjects. **IEEE Trans Med Imaging 18:**909–916, 1999

10. Dormont D, Ricciardi KG, Tandé D, Parain K, Menuel C, Galanaud D, et al: Is the subthalamic nucleus hypointense on T2-weighted images? A correlation study using MR imaging and stereotactic atlas data. **AJNR Am J Neuroradiol 25:**1516–1523, 2004

11. Finnis KW, Starreveld YP, Parrent AG, Sadikot AF, Peters TM: Three-dimensional database of subcortical electrophysiology for image-guided stereotactic functional neurosurgery. **IEEE Trans Med Imaging 22:**93–104, 2003

12. Fischl B, Salat DH, Busa E, Albert M, Dieterich M, Haselgrove C, et al: Whole brain segmentation: automated labeling of neuroanatomical structures in the human brain. **Neuron 33:**341–355, 2002

13. Ganser KA, Dickhaus H, Metzner R, Wirtz CR: A deformable digital brain atlas system according to Talairach and Tournoux. **Med Image Anal 8:**3–22, 2004

14. Gonzalez Ballester MA, Zisserman A, Brady M: Segmentation and measurement of brain structures in MRI including confidence bounds. **Med Image Anal 4:**189–200, 2000

15. Guo T, Finnis KW, Parrent AG, Peters TM: Visualization and navigation system development and application for stereotactic deep-brain neurosurgeries. **Comput Aided Surg 11:**231–239, 2006

16. Hamel W, Fietzek U, Morsnowski A, Schrader B, Herzog J, Weinert D, et al: Deep brain stimulation of the subthalamic nucleus in Parkinson's disease: evaluation of active electrode contacts. **J Neurol Neurosurg Psychiatry 74:**1036–1046, 2003

17. Kikinis R, Shenton ME, Iosifescu DV, McCarley RW, Saiviroonporn P, Hokama H, et al: A digital brain atlas for surgical planning, model driven segmentation and teaching. **IEEE Trans Vis Comput Graph 2:**232–241, 1996

18. Lehericy S, Bardinet E, Tremblay L, Van de Moortele PF, Pochon JB, Dormont D, et al: Motor control in basal ganglia circuits using fMRI and brain atlas approaches. **Cereb Cortex 16:**149–161, 2006

19. Mai JK, Assheuer J, Paxinos G: **Atlas of the Human Brain.** New York: Academic Press, 1997

20. Mallet L, Schupbach M, N'Diaye K, Remy P, Bardinet E, Czernecki V, et al: Stimulation of subterritories of the subthalamic nucleus reveals its role in the integration of the emotional and motor aspects of behavior. **Proc Natl Acad Sci U S A 104:**10661–10666, 2007

21. Mangin JF, Poupon F, Duchesnay E, Riviere D, Cachia A, Collins DL, et al: Brain morphometry using 3D moment invariants. **Med Image Anal 8:**187–196, 2004

22. Morel A, Magnin M, Jeanmonod D: Multiarchitectonic and stereotactic atlas of the human thalamus. **J Comp Neurol 387:**588–630, 1997

23. Niemann K, Mennicken VR, Jeanmonod D, Morel A: The Morel stereotactic atlas of the human thalamus: atlas-to-MR registration of internally consistent canonical model. **Neuroimage 12:**601–616, 2000

24. Niemann K, Naujokat C, Pohl G, Wollner C, von Keyserlingk D: Verification of the Schaltenbrand and Wahren stereotactic atlas. **Acta Neurochir (Wien) 129:**72–81, 1994

25. Niemann K, van Nieuwenhofen I: One atlas—three anatomies: relationships of the Schaltenbrand and Wahren microscopic data. **Acta Neurochir (Wien) 141:**1025–1038, 1999

26. Nowinski WL, Belov D, Pollak P, Benabid AL: Statistical analysis of 168 bilateral subthalamic nucleus implantations by means of the probabilistic functional atlas. **Neurosurgery 57:**319–330, 2005

27. Nowinski WL, Fang A, Nguyen BT, Raphel JK, Jagannathan L, Raghavan R, et al: Multiple brain atlas database and atlas-based neuroimaging system. **Comput Aided Surg 2:**42–66, 1997

28. Nowinski WL, Thirunavuukarasuu A: Atlas-assisted localization analysis of functional images. **Med Image Anal 5:**207–220, 2001

29. Pitiot A, Delingette H, Thompson PM, Ayache N: Expert knowledge-guided segmentation system for brain MRI. **Neuroimage 23 (1 Suppl):**S85–S96, 2004

30. Pollo C, Villemure JG, Vingerhoets FJ, Ghika J, Maeder P, Meuli R: Magnetic resonance artifact induced by the electrode Activa 3389: an in vitro and in vivo study. **Acta Neurochir (Wien) 146:**161–164, 2004

31. Prima S, Ourselin S, Ayache N: Computation of the mid-sagittal plane in 3D brain images. **IEEE Trans Med Imaging 21:**122–138, 2002

32. Saint-Cyr JA, Hoque T, Pereira LC, Dostrovsky JO, Hutchison WD, Mikulis DJ, et al: Localization of clinically effective stimulating electrodes in the human subthalamic nucleus on magnetic resonance imaging. **J Neurosurg 97:**1152–1166, 2002

33. Schaltenbrand G, Wahren W: **Atlas for Stereotaxy of the Human Brain.** Stuttgart: Georg-Thieme-Verlag, 1977

34. Shen D, Herskovits EH, Davatzikos C: An adaptive-focus statistical shape model for segmentation and shape modeling of 3-D brain structures. **IEEE Trans Med Imaging 20:**257–270, 2001

35. St-Jean P, Sadikot AF, Collins L, Clonda D, Kasrai R, Evans AC, et al: Automated atlas integration and interactive three-dimensional visualization tools for planning and guidance in functional neurosurgery. **IEEE Trans Med Imaging 17:**672–680, 1998

36. Stefanescu R, Pennec X, Ayache N: Grid powered nonlinear image registration with locally adaptive regularization. **Med Image Anal 8:**325–342, 2004

37. Talairach J, Tournoux P: **Co-planar Stereotaxic Atlas of the Human Brain**. New York: Thieme Medical Publishers, Inc., 1988

38. Xu M, Nowinski WL: Talairach-Tournoux brain atlas registration using a metalforming principle-based finite element method. **Med Image Anal 5:**271–279, 2001

39. Yelnik J, Bardinet E, Dormont D, Malandain G, Ourselin S, Tandé D, et al: A three-dimensional, histological and deformable atlas of the human basal ganglia. I. Atlas construction based on immunohistochemical and MRI data. **Neuroimage 34:**618–638, 2007

40. Yelnik J, Damier P, Demeret S, Gervais D, Bardinet E, Bejjani BP, et al: Localization of stimulating electrodes in patients with Parkinson disease by using a three-dimensional atlas-magnetic resonance imaging coregistration method. **J Neurosurg 99:**89–99, 2003

41. Yoshida M: Creation of a three-dimensional atlas by interpolation from Schaltenbrand-Bailey's atlas. **Appl Neurophysiol 50:**45–48, 1987

Address correspondence to: Jérôme Yelnik, M.D., Institut National de la Santé et de la Recherche Médicale U679, Hôpital de la Salpêtrière, 47, Boulevard de l'Hôpital, 75013, Paris, France. email: jerome.yelnik@upmc.fr.